The following supplements accompany the article

Dodging the blades: new insights into three-dimensional space use of offshore wind farms by lesser black-backed gulls *Larus fuscus*

Chris B. Thaxter*, Viola H. Ross-Smith, Willem Bouten, Elizabeth A. Masden, Nigel A. Clark, Greg J. Conway, Lee Barber, Gary D. Clewley, Niall H.K. Burton

*Corresponding author: chris.thaxter@bto.org

Marine Ecology Progress Series 587: 247–253 (2018)

Supplement 1. Additional information on data collection and analysis

Catching and tagging birds

South Walney is part of the Morecambe Bay and Duddon Estuary potential Special Protection Area (pSPA). This colony has reduced in size from 19,487 Apparently Occupied Nests (AONs) in 1998-2002 to 2,312 AONs in 2014 (JNCC 2016). Individuals were caught at the nest site during early incubation between 16 and 20 May 2014 using a walk-in wire mesh trap, and GPS devices were attached to 24 birds using a cross-over wing harness (Thaxter et al. 2015). The GPS tracking system, manufactured by the University of Amsterdam, consisted of a solar-powered GPS device, a laptop and base station, and a series of relays to facilitate remote download of data (Bouten et al. 2013). Three different models of GPS device were used, with equivalent functionality but varying in weight (Model 5CDL, 13.5 g, n = 10 birds; Model 4CDL, 15.5 g, n = 5 birds; and 4CDL 18.5 g, n = 9 birds). The maximum weight of devices (plus harness) was 20.5g (< 3% body mass in all cases, mean body weight = 806±94 g, range, 640-1060 g). Birds in this study were sexed using head and bill length measurements recorded along with body mass on capture (Coulson et al., 1983; Camphyusen, 2011). The 2 example birds presented in the main paper (4032 and 5026) were female and male respectively.

Wind farm information used in this study

This study uses acronyms to describe spaces of interest within 1D, 2D and 3D space. Specifically, these are: (1) the 1D vertical rotor swept zone (vRSZ), i.e. the zone between the upper and lower points swept by the rotor blades (equating to a collision risk window), (2) the 2D horizontal swept zone (hRSZ), equating to the maximum distance away from the turbine swept by the rotors (i.e. the rotor's radius), and (3) the 3D rotor swept volume (RSV). A schematic representation of these spaces is provided in Fig. S1 below. The distance to nearest turbine is presented in Fig. S1 as an expression (integral) of the 2D xy horizontal space. Note also that turbine orientation is excluded from this calculation; in reality, the hRSZ is likely to be a collection of 1D horizontal planes specific to individual turbines. Our approach to avoidance is therefore precautionary.

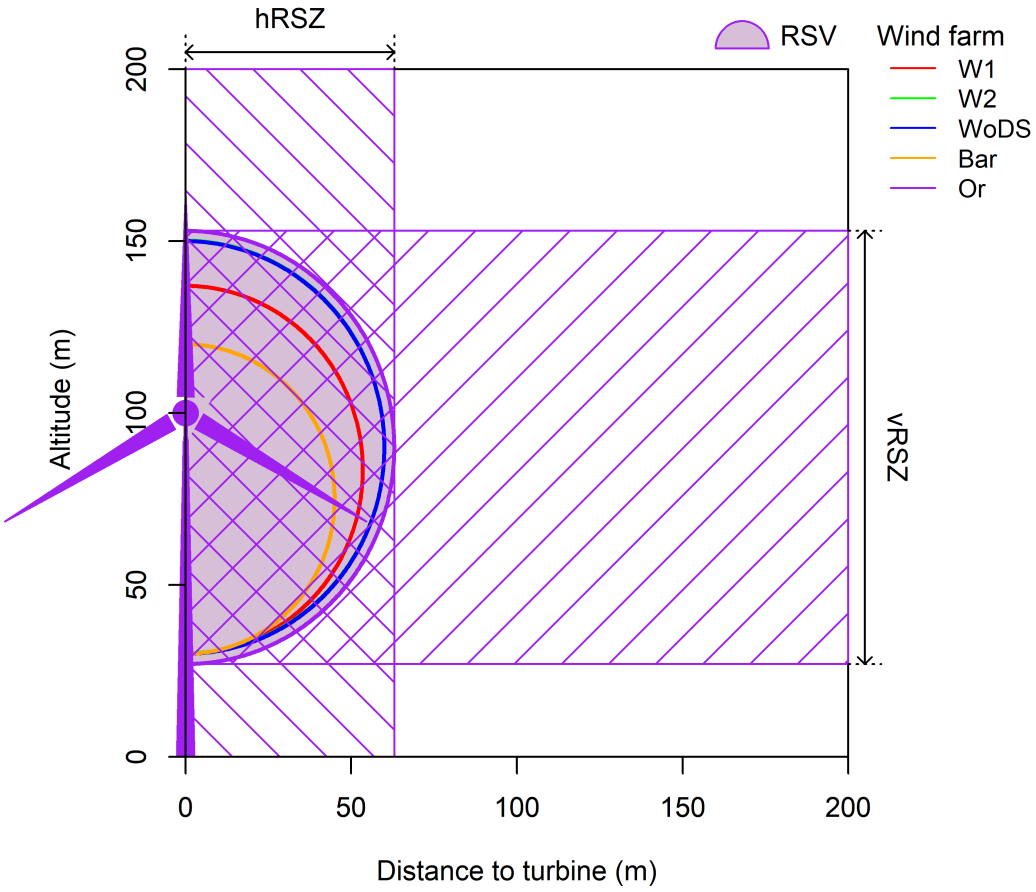

Fig. S1. Schematic representation of a single turbine and definitions of the horizontal rotor swept zone (hRSZ), vertical rotor swept zone (vRSZ), the latter equating to a collision risk window, and the three-dimensional rotor swept volume (RSV), depicted here as a 2D area over distance to nearest turbine, for the OWF with the largest turbines in the study area, Ormonde (Or); other RSVs are also depicted for the Walney 1 (W1), Walney 2 (W2), West of Duddon Sands (WoDS) and Barrow (Bar) OWFs; note W2 and WoDS have near identical vRSZs.

In this study, we initially separated GPS fixes into those within OWFs and those locations outside. The perimeter of each wind farm was delineated by the shape formed by the outermost turbines, including a buffer of 63 m equating to the maximum horizontal turbine swept zone of any individual OWF in the study area (4C Offshore 2017). The vRSZ in this study was given as 30-120 m, 27-153 m, 30-137 m, 30.2-150.2 m and 30-150 m, for the Barrow, Ormonde, Walney 1, Walney 2, and West of Duddon Sands OWFs respectively (4C Offshore 2017), and hRSZ were thus respectively 45 m, 63 m, 53.5 m, 60 m and 60 m. These turbine characteristics were used for bespoke assessments of RSV overlaps in final conclusions (see Fig. S1).

Analytical details

To assess the time spent within OWFs, temporal overlaps was estimated by linear interpolation of tracks to 1 s, and calculating the time elapsed between OWF entry and exit points. To assess two-dimensional space use, flight altitudes were plotted as a kernel density

histogram, with the smoothing parameter based on the mean of the normal optimal values (Bowman and Azzalini 1997). To assess the 3-dimensional spatial volume usage and indicate concentrations of use, we computed utilisation distributions using a bivariate normal kernel taking a normal reference bandwidth (Venables & Ripley 2002). To assess the relative use of the RSV in relation to a null distribution, we used a resampling approach to randomly distribute points within the horizontal plane. Tests were performed on data collected at 10 second sampling intervals (4032, n = 4,305; 5026, n = 1,744), as well as data sub-sampled to one fix every five minutes (4032, n = 484; 5026, n = 1,425) and one fix every hour (4032, n = 41; 5026, n = 209); the latter ensured removal of a temporal autocorrelation bias in the data (e.g. Ross-Smith et al. 2016). Note also that bird 4032 had more data at the finest resolution of 10 seconds than bird 5026, but bird 5026 had more data at five minutes (see also Table S2). The proportion of observed fixes within the RSV was compared with the null pattern using a paired t-test, for data collected at intervals of 10 seconds, and data sub-sampled to one fix every five minutes and 60 minutes (Supplement 2), accounting for temporal autocorrelation (Ross-Smith et al. 2016).

The proportion of fixes within the RSV was found to be significantly lower than a random distribution for sampling rates of 10 seconds (difference, 0.19, 95% CI 0.19-0.21; $t = 65.6$, $p < 0.001$), five minutes (0.20, 0.17-0.21; $t = 27.5$, $p < 0.001$) and 60 min (0.43, 0.39-0.47; $t = 22.1$, $p < 0.001$).

References

4C Offshore (2017) 4C Offshore. www.4coffshore.com/offshorewind (accessed 28 July 2017)

Bowman AW, Azzalini A (1997) Applied smoothing techniques for data analysis: the kernel approach with S-Plus illustrations. Oxford Univ Press, UK

Camphyusen CJ (2011) Lesser black-backed gulls nesting at Texel foraging distribution, diet, survival, recruitment and breeding biology of birds carrying advanced GPS loggers. NIOZ-Report 2011-05, Royal Netherlands Institute for Sea Research, Texel.

Coulson JC, Thomas CS, Butterfield JEL, Duncan N, Monaghan PC (1983) The use of head and bill length to sex live gulls Laridae. Ibis 125: 549–557

JNCC (2016) Seabird Monitoring Programme online database www:/jncc.defra.gov.uk/smp (accessed 12 September 2016)

Thaxter CB, Ross-Smith VH, Bouten W, Clark NA, Conway GJ, Rehfisch MM, Burton NHK (2015) Seabird–wind farm interactions during the breeding season vary within and between years: A case study of Lesser black-backed gull *Larus fuscus* in the UK. Biol Conserv 186: 347–358

Venables WN, Ripley BD (2002) Modern applied statistics with S. Fourth edition. Springer.

Supplement 2. An appraisal of GPS altitude errors at different temporal sampling rates.

Introduction

Measurements of position taken by any tracking system are subject to a degree of error. In the context of wind farms and their potential impacts on wildlife, the measurement of altitude of airborne taxa such as birds and bats is crucial for collision risk modelling (Masden & Cook 2016). Where potential error biases may occur, they must therefore be understood, minimised and if possible accounted for to allow sound judgements on the likely risk posed by wind farms to be made.

Measurements of altitude in GPS systems are considered particularly error prone in terms of both precision (error around central estimate) and accuracy (deviation of the central estimate from the 'true' value). These errors may potentially arise from several different sources (Ross-Smith *et al*. 2016). At the outset, the satellite position itself above the earth is considered accurate to between *ca*. 1 and 5 m, and the atomic clocks on-board the satellites can also contain GPS time errors (e.g. 10 ns), in turn translated to a distance error at the earth's surface (ublox 2009, 2013). The ionosphere and troposphere, through which signals must travel, can also cause changes to the velocity of signals between satellites and receivers, for instance, due to ionisation of particles and changes in temperature and humidity. The GPS signals may potentially also be split into multiple paths, for example, as they reflect off infrastructure such as buildings, mountains and trees, giving rise to further error. Time delays and noise associated with the receiver, and variations in the ephemeris and almanac information used to assess the positioning of satellites can produce additional errors in precision (ublox 2009). Many of these error sources can be adjusted for, to a degree, through differential GPS systems, which determine correction factors based on additional reference stations; wide-scale applications include the Satellite Based Augmentation Systems that calculate the integrity of GPS and correction data on the ground, that are in turn broadcast back to the user through separate geostationary satellites (ublox 2013). Further, the GPS module used in tags in this study measures and calculates the distance from the satellite to itself and in turn, for positions at sea, calculates the height above mean sea level using the WGS84 worldwide datum, which based on ellipsoid representations of the earth, also contains some inaccuracy. For positions over land, corrections for topographical variations are then applied using a digital elevation model developed from the Shutter Radar Topography Mission (Farr et al. 2007) – although note in this study the focus was on offshore locations only.

Aside from the many factors noted above, the GPS receiver itself can give rise to additional precision errors in altitude measurements. A particular contributory factor here is the sampling frequency specified by the user in the software, and associated firmware settings that accompany these choices within the GPS module. Previous tests using the University of Amsterdam GPS tags, as used in the current study, have revealed that altitude precision is improved through an increased sampling frequency (Bouten *et al.* 2013; unpubl.). This is because the GPS module is powered up constantly for sampling intervals of up to 16 s, meaning that the receiver works at maximum capacity to achieve the greatest precision (ublox 2013). Selecting a five-minute GPS sample rate automatically switches the tag to an energy-saving interval mode (for all sampling greater than 16 s), which greatly slows down the receiving of ephemeris and almanac information used to process positional information. Consequently, altitude information from rates greater than 16 s are considered less precise for this system.

Methods

Here, we tested the data used in the present study for calculating flight altitudes. We quantified the degree of precision and accuracy surrounding the altitude data presented at different sampling rates for the two example birds 4032 and 5026. This test was based on locations when birds were expected to be resting on the sea surface and at mean sea-level, using travel speed to separate 'non-flight' ($\leq$ 4 km h^{-1}) activity from 'flight' (> 4 km h^{-1}) activity (Shamoun-Baranes et al. 2011). For this experiment we also examined GPS altitude measurements in relation to varying temporal GPS sampling rates of the tag. In this study we defined 'fast-sampling' observations as those collected at rates of less than 60 s, and provide a breakdown of number of fixes collected at different rates – see Table S2. For examination of three-dimensional patterns, we used data collected at 10 s rates to both maximise data availability and avoid unequal sampling and biases. As noted above, locations recorded at sampling intervals of less than or more than 16 s may be expected to be subject to different error, and consequently, the use of the 10 s data was expected to minimise precision errors. Here, we examine this prediction by quantifying the precision and accuracy of data grouped into different sampling rates. As detailed in Table S2, these were split into rates of 10, 16, 60 and 300 s (five minutes). We also filtered data by date-time to only included locations recorded within 2 hours of mid-tide, when it would be expected that fixes would be closest in altitude to zero, i.e. mean-sea level. Tide data were obtained from the British Oceanographic Data Centre (https://www.bodc.ac.uk/data/online_delivery/ntslf/), using the nearest tide gauge to the South Walney breeding colony [Heysham ~20 km, tidal range from 1 May 2014 to 1 September 2014: 6.8±1.4SD m (range, 3.7-9.8 m); diurnal cycle: 5.7±0.2SD h (range, 4.8-6.0 h)]. Tidal minimum and maximum values, were obtained using the R package 'Tides' (Cos & Schepers 2017), and mid points were estimated manually taking the linear mid-point time between high and low tide. We note, however, that within the four-hour period (two-hours either side of mid-tide), there was still a mean fluctuation in sea level of 2.9±0.6 m either side of mid-tide. Data are presented as frequency histograms. Box-and-whisker analysis was used to summarise the distributions based on the median (50% percentile), the interquartile range (upper quartile UQ, 75% percentile, lower quartile LQ, 25% percentile), and the upper and lower 'whiskers' of the distribution; here, the upper whisker is defined as the maximum point falling within 1.5*(UQ-LQ)+UQ, and the lower whisker as the minimum point falling within LQ-1.5*(UQ-LQ). For bird 5026, an additional complication arose with a set of stationary values clustered around 30 m, centred around static xy locations; although not confirmed, these points were very likely to be the bird perching on platforms at sea, such as oil rigs and met. masts. Therefore, we also identified these individual locations using GoogleEarth© and removed them from this assessment, so as to only include locations expected to be on the sea surface.

Results

The precision of GPS altitude measurements associated with data collected at the 300 s sampling rate was lower compared to that for data collected at 10, 16 s 60 s rates (Fig. S2, Table S1). Whisker ranges were greatest for data collected at the 300 s rate, particularly for bird 4032 (Table S1) and interquartile ranges generally increased with coarseness of sampling rate, although note that for bird 4032 the 60 s rate had greater precision error, albeit with fewer data points. The precision of GPS altitude measurements associated with data collected at 10 s and 16 s sampling rates was similar, with interquartile ranges and whisker ranges of GPS altitude measurements varying between 3-5 m and 10-16 m per bird, respectively. Interestingly, the medians and modes of the distributions for data collected at

rates of 10 s for both birds and 16 s for bird 5026 were 2-4 m above mean sea level indicating a likely accuracy bias of the altitude data, presumably due to the estimation/calculation in relation to the WGS84 ellipsoid or fluctuations within the mid-tide cycle as highlighted in the methods above.

Discussion

In summary, the central 75% spread of GPS altitude measurements associated with data collected at the 10 s sampling rate, as presented for the two example birds in this paper, was 3 and 4 m for birds 4032 and 5026 respectively, with a more conservative whisker ranges of 11 and 14 m. It is likely that most of the GPS locations were therefore suitably precise. This quality of data is also clearly visible in Fig. 3, where yellow resting locations were highly clustered around very low altitude – here determined as just above zero due to a slight accuracy bias. Consequently, it is deemed unlikely that the conclusions drawn in this paper are influenced by the precision of altitude information, particularly for overlaps with the three-dimension rotor swept zone, especially as very few locations were within the horizontal rotor swept zone of the turbines, regardless of altitude or bird behaviour. The error in both the precision and accuracy of GPS altitude measurements can be brought into the estimation of variation around flight height distributions, for example through Bayesian approaches (Ross-Smith et al. 2016), although the initial sample sizes in this paper prevented a more thorough modelling approach being applied.

Table S1. Boxplot results from the investigation of altitude measurements (m) from GPS tags attached to lesser black-backed gulls 4032 and 5026 at South Walney; data here are for locations at sea where birds were deemed to be resting on the sea surface, and within two hours of mid-tide. Data collected at sampling rates of 10-16 s (best data resolution), 10-60 s (maximal use of all 'faster sampling' locations) and 300 s (where tags were programmed solely to an energy-saving interval mode). Boxplot statistics are also shown for each frequency histogram presented in Fig. S2.

		Sampling rate			
Bird	**Level**	**10 s**	**16 s**	**60 s**	**300 s**
4032	No. points	7433	419	53	676
	Lower whisker (m)	-2	-7	-13	-10
	Lower quartile (m)	2	-2	-5	-1
	Median (m)	3	0	0	2
	Mode (m)	2	0	0	0
	Upper quartile (m)	5	3	3	5
	Upper whisker (m)	9	9	9	14
	Inter-quartile range (m)	**3**	**5**	**8**	**6**
	Whisker range (m)	**11**	**16**	**22**	**24**
5026	No. points	553	223	120	1972
	Lower whisker (m)	-3	0	-7	-7
	Lower quartile (m)	1	3	-2	0
	Median (m)	2	4	0	2
	Mode (m)	2	4	0	0
	Upper quartile (m)	5	6	2	5
	Upper whisker (m)	11	10	6	12
	Inter-quartile range (m)	**4**	**3**	**4**	**5**
	Whisker range (m)	**14**	**10**	**13**	**19**

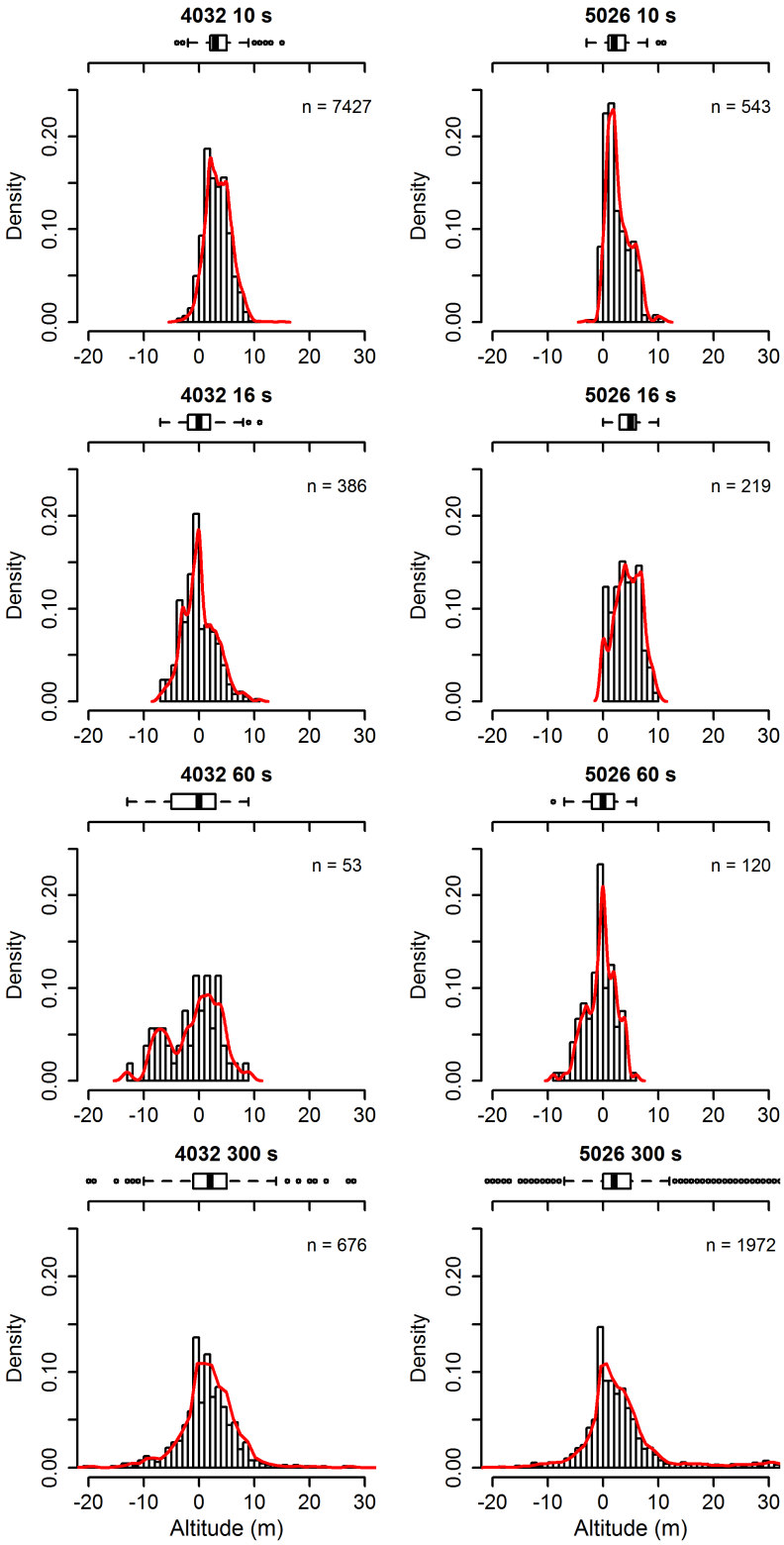

Fig. S2. Frequency histograms and boxplots from the investigation of altitude measurements (m) from GPS tags attached to lesser black-backed gulls 4032 and 5026 at South Walney at varying sampling rates (see text); data here are for locations at sea where birds were deemed to be resting on the sea surface, and within two hours of mid-tide.

References

Cox T & Schepers L (2017) Tides: Quasi-Periodic Time Series Characteristics. R package version 2.0. http://CRAN.R-project.org/package=Tides

Farr TG, Rosen PA, Caro E, Crippen R, Duren R, Hensley S, Kobrick M, Paller M, Rodriguez E, Roth L, Seal D, Shaffer S, Shimada J, Unland J, Werner M, Oskin M, Burbank D, Alsdorf D (2007) The Shuttle Radar Topography Mission. Rev Geophys: 45 RG2004. doi:10.1029/2005RG000183

Masden EA & Cook ASCP (2016) Avian collision risk models for wind energy impact assessments. Science Direct 56: 43-49.

Michelot T, Langrock R, Patterson T & Rexstad E (2015) moveHMM. An R package for animal movement modelling

Shamoun-Baranes J, Bouten W, Camphuysen CJ, Baaij E (2011) Riding the tide: intriguing observations of gulls resting at sea during breeding. Ibis 153: 411–415

Shamoun-Baranes J, Bouten W, van Loon EE, Meijer C & Camphuysen CJ (2016) Flap or soar? How a flight generalist responds to its aerial environment. Phil Trans Roy Soc B 371: 20150395

Ross-Smith VH, Thaxter CB, Masden EA, Shamoun-Baranes J, Burton NHK, Wright LJ, Rehfisch MM & Johnston A (2016) Modelling flight heights of lesser black-backed gulls and great skuas from GPS: a Bayesian approach. J Appl Ecol 53: 1676–1685

ublox (2009) GPS Essentials of Satellite Navigation Compendium, GPS-X-02007-D. https://www.u-blox.com/sites/default/files/products/documents/GPS-compendium_Book_%28GPS-X-02007%29.pdf (accessed 13 October 2017)

ublox (2013). u-blox 6 Receiver Description Including Protocol Specification, GPS.G6-SW-10018-F. https://www.u-blox.com/sites/default/files/products/documents/u-blox6_ReceiverDescrProtSpec_%28GPS.G6-SW-10018%29_Public.pdf (accessed 13 October 2017)

Supplement 3. Representativeness of fast-sampling data

The data presented in this study included movement locations sampled every five minutes as a standard baseline rate, interspersed with periods of faster sampling between 10 s and 60 s, (Table S2), when tags were in 'energy-surplus' mode. The energy surplus mode was switched off when the battery was below 3.95 V but commenced again when charged above 4.05 V. Such faster rates were only possible during the day when enough light was available to power the solar panels – a greater amount of cloud cover reduced the capacity for faster sampling rates. Here, we assume that faster sampling rates were representative of daytime behaviour when assessing 3-dimensional space use. The 3-dimensional volume use and overlap with the RSV was assessed using data collected at 10 s intervals (Fig. 3); for birds 4032 and 5026, 88% and 54% of fixes collected by these birds within OWFs were at 10 s rates, the remainder being fixes collected at coarser sampling intervals (Table S2). However, it is possible that bird behaviour may be affected between different weather conditions (Shamoun-Baranes et al. 2006). Here, we assess this potential bias by filtering the fast-sampling data to 5 minutes, and combining it with the data that were only collected on a 5-minute rate (i.e. when fast sampling was not possible), thus giving an unbiased dataset to any particular time of the day or conditions. This same approach is used to assess distributions of flight altitudes within/outside OWFs for day/night periods (Fig. 2). Data were subset for daytime only periods to compare to the fast-sampling data collected over the same diurnal period. The same kernel density plot of distance to nearest turbine against altitude was then plotted.

Table S2. Summary of number of fixes available for assessment of behaviour within and outside wind farms for both day and night periods under different sampling rates. Sexes are also presented with parentheses denoting likely but less certain sex. Note, further fixes were collected at coarser rates of 30 mins at the end of the season in preparation for birds departing for the non-breeding period, but are not presented here.

		Outside wind farm								**Inside wind farm**							
		Day				**Night**				**Day**				**Night**			
Bird	**Sex**	**10 s**	**16 s**	**60 s**	**300 s**	**10 s**	**16 s**	**60 s**	**300 s**	**10 s**	**16 s**	**60 s**	**300 s**	**10 s**	**16 s**	**60 s**	**300 s**
494	(M)	1		44	145				53			38	65				111
496	F			6	12				24			2	4				3
497	M								15								
499	M	26	79	123	512	1			421				129				111
501	M	18	110	36	436	1			435	5	38	4	52				50
502	M			1	3												
503	F	25	101	134	217	1			165								
504	F	22	145	508	1615				349			1	8				
506	(M)	5	4	210	863	3			732	1	1	10	234				167
4031	M	5933	1375	643	308	10		13	157	258	14		17				26
4032[a]	F	14877	1076	33	796	42	10		812	4249	241	4	232	56	1		108
4033	(M)	9	127	13	23	1			17								
4034	M	1	30	2	16				114								
4035	(M)	84	4141	232	480	1	84	8	456		7						
5023	F	1	1		15	2			225								
5024	(M)	1969	1169	56	509	1			620	154	246	2	123				326
5025	M	2010	3761	3438	1932	3			629		59		1				
5026[a]	M	3487	454	155	2519	1			1599	1744	513	132	625				585
5027	M		1		1				123								
5029	F	1	3	8	10	2			39								
5030	M	6857	1293	36	184	11	62	2	302		2	6	1				
5032	F	438	548	65	30	1	9		95		32	1					
5033	F	1597	2861	108	118	142	2	1	171								
5034	M	3793	856	342	141	2			107	56	33	1	4				

[a] Birds 4032 and 5026 were selected for additional investigation into fine-scale space use

Fig. S3 shows that the dataset filtered to 5 minutes gave a broadly similar pattern to the fast-sampling data as shown in Fig. 3 of the main paper. Overlaps with the RSV were also very similar, and the central core of the kernel distributions was at equivalent distances from nearest turbines and in the vertical dimension. For 5026, an additional lesser core was also seen at a lower altitude beneath the vRSZ (see also Fig. 2 of the main paper), but the main concentration of locations at higher altitudes was highly congruent with the fast sampling data. For both birds, a greater number of fixes below zero highlighted the greater potential error surrounding data with wider sampling intervals. This test therefore confirmed the fast-sampling data presented in the main paper were broadly representative of daytime space use within the wind farm. Note, however, this cannot be used to confirm that behaviour was unaffected by different conditions, since the correlation between the general use of offshore areas and environmental conditions was not assessed within this study.

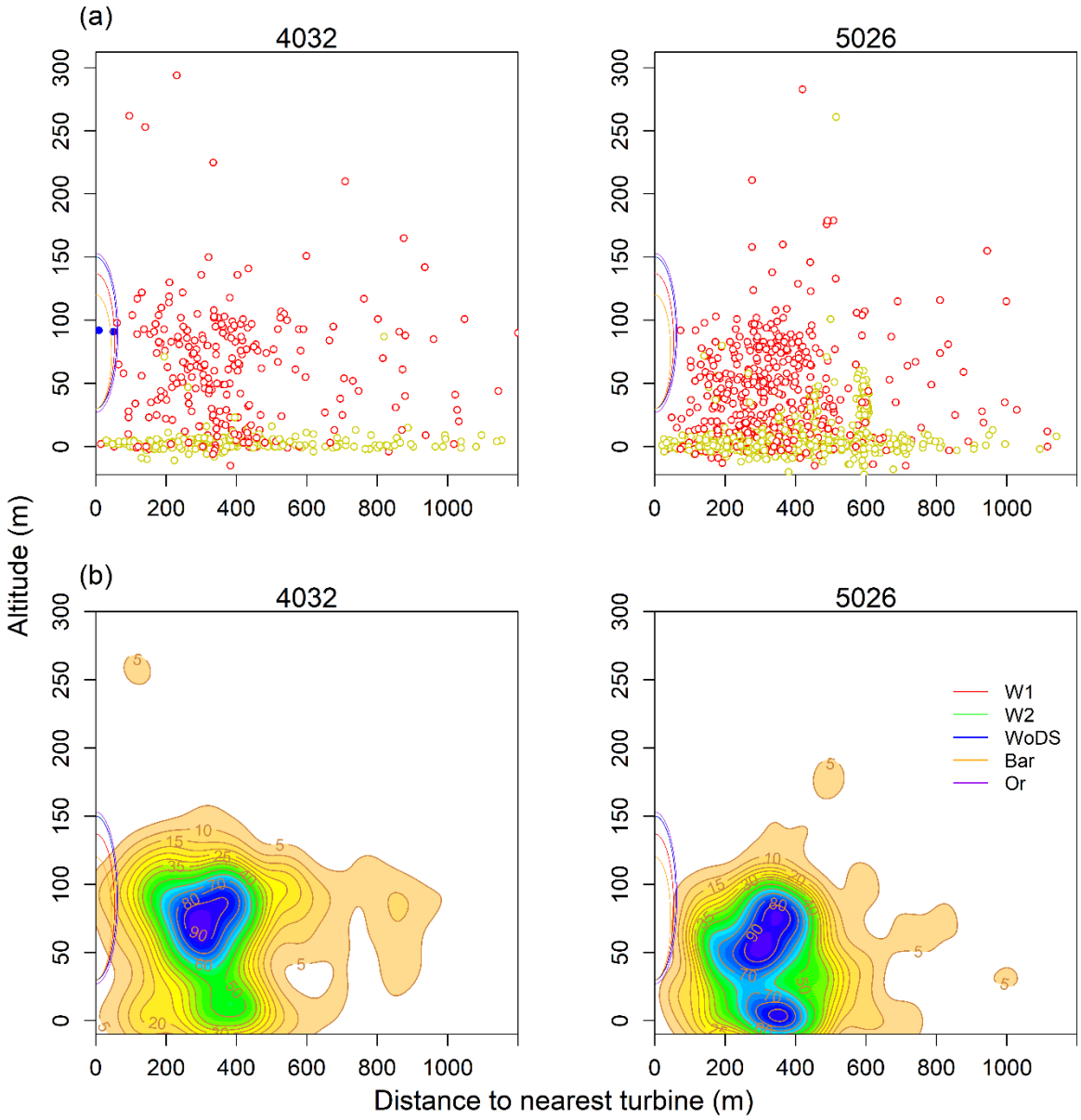

Fig. S3. Distributions of fixes of 2 *Larus fuscus* (left panels: Bird 4032; right panels: Bird 5026) within operational offshore wind farms (OWFs) during the daytime period based on data filtered to a rate of 300 s (5 mins). Horizontal axes show distance from the nearest wind

turbine; vertical axes show flight altitude (m). Coloured curves adjacent to the y-axes indicate 3-dimensional rotor swept volumes (RSVs) of the 5 operational OWFs in the area: Walney 1 (W1), Walney 2 (W2), West of Duddon Sands (WoDS), Barrow (Bar) and Ormonde (Or) (see inset key to colours; for locations see www.4coffshore.com/offshorewind). (a) Distance to nearest turbine and altitude for flight (red; travel speed > 4 km h^{-1}) and resting, bathing or swimming (yellow; travel speed ≤ 4 km h^{-1}) Solid points indicate overlaps with RSVs; the colour identifies the wind farm concerned. (b) Kernel density estimation of fixes of birds in flight illustrating overlaps with the RSV determined using the 95% KDE (i.e. the area of overlap with the 5% contour line)